Li concentration dependence of structural properties and optical band gap of Li-doped ZnO films

Karima Meziane[1] · **Ahmed El Hichou**[1] · **Asmae El Hamidi**[1] · **Mostafa Chhiba**[2] ·
Abdellatif Bourial[3] · **Abdelmajid Almaggoussi**[1]

Abstract Li-doped and undoped Zinc oxide thin film by the sol–gel method and spin-coated on glass substrate, and the effect of doping on structural, optical and stress properties have been investigated. X-ray diffraction analysis showed that all the films are polycrystalline with a hexagonal wurtzite structure. For a low amount of Li up to 12%, the texture coefficient increases with the Li amount ensuring an improvement of the c-axis orientation and the crystallinity. The crystallite size seems slightly affected and ranged in the nanometer range. Beyond this, Li amount value, the texture coefficient decreases drastically showing deterioration in the growth of ZnO along c-axis. Scanning electron microscopy (SEM) images show that the morphology of films was highly influenced by Li incorporation. For Li amount exceeding 12%, SEM images show the appearance of some cracks. The optical results revealed an improvement of the total transmission when increasing the Li amount up to 12%. A linear decrease of band gap energy with the Li content was observed. The stress was calculated and found depending on the Li amount analogously to the band gap energy. Thus, the band gap energy and the stress are correlated.

✉ Ahmed El Hichou
a.elhichou@uca.ma; aelhichou@yahoo.fr

1   Groupe d'Étude des Matériaux Optoélectroniques (G.E.M.O), Faculté des Sciences et Techniques, Université Cadi Ayyad, Av.A. ElKhattabi, BP 549, 40000 Marrakech, Morocco

2   Laboratoire Rayonnement Matière et Instrumentation, Faculté des Sciences et Techniques, Université Hassan 1, 26000 Settat, Morocco

3   Laboratoire Procédés, Métrologie, Matériaux pour l'Énergie et Environnement (LP2M2E), Faculty of Sciences and Techniques, Department of Applied Physics, Cadi-Ayyad University, A.El Khattabi, Marrakech, Morocco

1 Introduction

Zinc oxide (ZnO) is a hexagonal wurtzite structure semiconductor mostly used in nanotechnology. This material is very interesting for many applications because of its wide direct band gap, $E_g = 3.37$ eV at room temperature, associated with a high exciton binding energy 60 meV [1, 2]. ZnO is intensively used as a transparent electrode in solar cells [3, 4], piezoelectric nanogenerator [5], chemical and gas sensors [6, 7], spintronic devices, and light emitting diodes [8, 9]. Zinc oxide under different morphologies can be prepared by various deposition techniques such as rf sputtering [10], chemical vapor deposition [11], pulsed laser deposition [12], spray pyrolysis [13], molecular beam epitaxy [14] and so forth. Besides these methods, the sol–gel process and spin-coating technique have attracted considerable attention. Its advantages include the relative simplicity and the feasibility to produce large area films without the need for an ultra-high vacuum and the produced films can be controlled step by step. The deposition temperatures are considerably lower than in many other methods. These features make spin-coating a low-cost deposition method.

An effective process for manipulating the physical properties of semiconductors involves impurity doping. Many works have been reported on the doping of ZnO with a wide variety of ions to meet the demands of several applications. Typical dopants that have been used to produce conducting films of ZnO belong to the group III elements (B, Al, In, Ga) and IV elements (Pb, Sn) of the periodic table, although there are many studies concerning physical properties of ZnO doped with lithium (Li). Lithium has been an important impurity in ZnO. It is effective to enhance the crystal growth rate due to increase in diffusivity [15] and it is also a deep acceptor and

changes the conductivity of the n-type material to semi-insulating [16].

Wang et al. [17] deposited Li-doped ZnO thin films with the sol–gel method. They reported that the films had polycrystalline wurtzite structure and high c-axis preferred orientation (002). Majumdar and Banerji [18] reported the structural and optical properties of Li-doped ZnO at different contents of Li incorporation in ZnO by the sol–gel method. They found that the crystalline structure of the films had wurtzite structure of the lattice and had 3.36 eV band gap value. Xiao et al. [19] deposited Li-ZnO thin films by using pulsed laser deposition. They reported that the thin films had the preferred (002) growth orientation and high transmittance (about 90%) in visible region at different substrate temperatures. Mohamed et al. [20] deposited Li-ZnO thin films by DC magnetron sputtering method on sapphire. They measured the transmission and reflection spectra and determined the absorption coefficient, optical band gap films at room temperature. The films showed the direct allowed optical transitions.

In the present work, lithium-doped and undoped ZnO thin films were synthesized by the sol–gel method using highly alkaline sols. The structural, morphological and optical properties have been investigated versus lithium content. In addition, we report the influence of stress on band gap.

2 Experimental details

All chemicals products (Aldrich 99%) for this research were of analytical grade and used without further purification. ZnO thin films were prepared by the sol–gel method and deposited on glass substrates by spin-coating technique. The lithium nitrate (LiNO3) and zinc acetate dehydrate (Zn $(CH_3COO)_2$, $2H_2O$) were used as a source of doping and precursor, respectively. 2-Methoxy ethanol was the solvent and monoethanolamine (MEA) was the stabilizing agent. First, 0.6 mol/l of zinc acetate and the desired lithium nitrate concentration were dissolved in a mixture of 20 ml of 2-methoxy ethanol and MEA. To obtain a clear, transparent and homogenous solution, the molar ratio of MEA to zinc acetate (ZnAc/MEA) was fixed as 1:1. The obtained sols were stirred at 80 °C for 2 h. Then the ammonia (NH_3) was gradually added in order to get the pH = 10 [21].

After that, the solution was kept still for 24 h, the sol was dropped on the glass substrate and spin-coated. To evaporate the solvent, the substrates were kept at 150 °C for 15 min in a tube furnace. This procedure was repeated ten times to obtain the desired thickness. Afterwards, the films were annealed at 500 °C for 90 min in order to eliminate the organic component in films.

X-ray diffraction (DRX) measurements were realized using Bragg–Brentano geometry [Bruker D8 Advance, Cu Kα radiation ($\lambda = 1.5418$ Å)]. The morphology of the films was studied using a field emission scanning electron microscope (FE-SEM) (JEOL J7600F). The SEM images were acquired with a fixed electron beam at low accelerating voltage (10 kV).

For optical studies, a computer-controlled UV–Vis–NIR spectrometer (Shimadzu UV-3101PC) was used in the spectral range 250–2200 nm. Blank glass substrate was used as reference for transmittance measurements.

The thickness of the all films was measured through a profilometer (Taylor Hobson precision Form Talysurf 50 with μltra software), with an accuracy to the height of 16 nm. The thickness was ranged around 200 nm.

3 Results and discussion

3.1 Structural and morphological properties

Figure 1 shows the DRX of undoped and lithium-doped ZnO thin films with various Li contents. The presence of several peaks in the DRX data reveals that all films are polycrystalline with a hexagonal wurtzite-type structure. The corresponding diffraction patterns exhibit three main diffraction peaks: (100), (002) and (101) corresponding to 2θ values of 31.79°, 34.46° and 36.22°, respectively. Minor diffraction lines (102), (110), (103) and (112) belonging to the ZnO structure were also detected and have a low intensity. Indeed, according to the JCPDS data (36-1451), the X-ray diffraction patterns confirm that the thin films synthesized in this study are ZnO with typical diffraction peaks of hexagonal (wurtzite) ZnO. No diffraction peak related to Li or Li compound is observed at different doping levels, indicating that Li substituted Zn or incorporated into interstitial sites in the ZnO lattice.

From the evolution of the diffraction pattern with the doping amount in the sample, it can be observed that the quantity of Li doping influences the growth orientation of the crystals. We have found that (002) and (101) peaks manifest close intensities and therefore no preferential orientation is observed for undoped ZnO. When the lithium is introduced, the DRX data reveal that there is only one main orientation (002) of Li-ZnO up to 12% Li concentration. The high intensity of (002) reflection compared with the relative weak (100) and (101) reflections suggests that the films exhibit a preferential c-axis orientation up to 12% of Li doping. The intensity of the diffraction peak (002) decreases by increasing the concentration of Li up to 12% and becomes of the same order of magnitude with the diffraction peaks (101). The intensity of the peaks demonstrates high purity of the

Fig. 1 XRD patterns of the Li-doped ZnO thin films deposited on glass substrates by sol
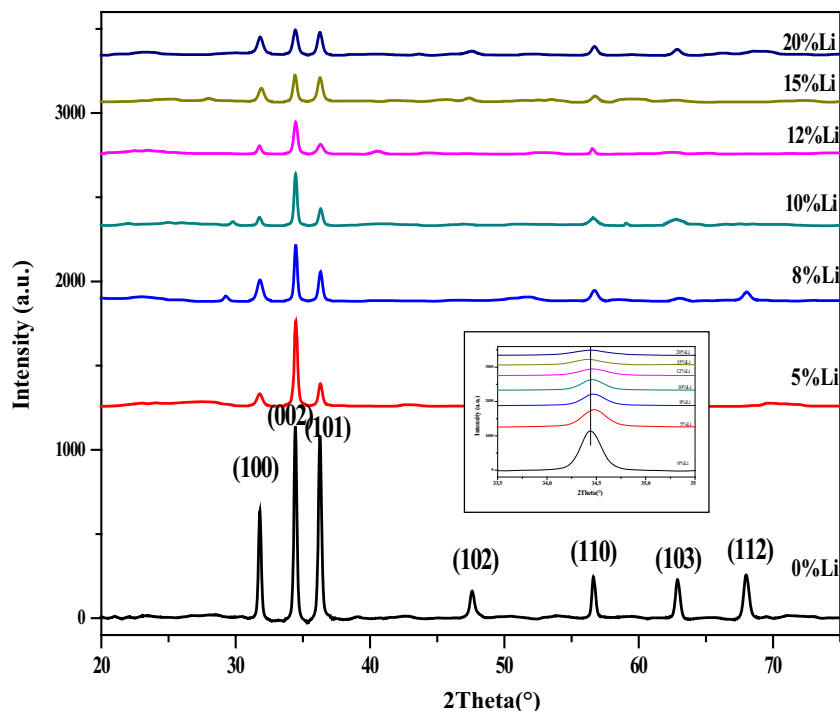
hexagonal ZnO phase and high quality of crystallinity of the samples up to 12% Li amount.

The lattice parameters *a* and *c*, the texture coefficient and the average crystallite size were calculated for all samples and tabulated (Table 1). It was found that the introduction of small amount of Li (5%) has no effect on the parameter a, whereas a decrease in the parameter c was detected. Senol et al. [22] reported the same result. This decrease in lattice parameter has resulted in the (002) peak shift to higher 2θ as shown by the insert in Fig. 1. This indicates that the doping atoms were incorporated into ZnO thin films and Li lodged itself in an interstitial position, which leads to a decrease of the lattice constants. This result indicates that an excess increase in doping concentration deteriorates the crystallinity of films, which may be due to the formation of stress by the difference in ionic radii between Zn (0.074 nm) and Li (0.068 nm).

For Li-doped ZnO and for doping contents up to 12%, both *c* and *a* unit cell parameters are almost constant giving a *c/a* ratio close to 1.6. When the Li content exceeds 12%, the parameter *a* decreases, while the parameter *c* increases. The *c/a* ratio does not undergo any significant change reflecting the maintained good compactness. This is reinforced by the higher values of texture coefficient Tc obtained for Li contents up to 12%, and its sharp decrease beyond this value as seen in Fig. 2. The higher values of Tc reveal that the ZnO films crystallinity is improved after introducing Li concentration up to 12%. The decrease of Tc is due to the decrease in mobility of Zn and O atoms with increasing Li concentration over 12%, which leads to a change of the preferred growth orientation.
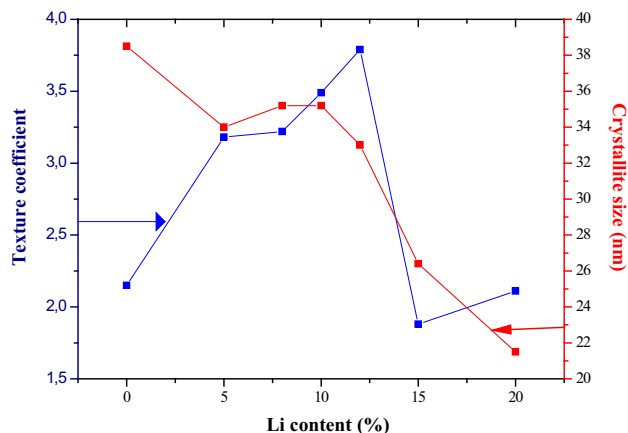
Table 1 Structural parameters of undoped and Li-doped ZnO thin films obtained by sol gel method

Sample	Li content	*a* (Å)	*c* (Å)	Tc (002)	*D* (nm)
0LZO	0	3.2518	5.2116	2.15	38.490
5LZO	5%	3.2529	5.2064	3.18	34.535
8LZO	8%	3.2511	5.2074	3.22	35.219
10LZO	10%	3.2542	5.2092	3.49	35.219
12LZO	12%	3.2547	5.2083	3.79	32.401
15LZO	15%	3.2406	5.2152	1.88	26.401
20LZO	20%	3.2488	5.2116	2.11	21.505

Fig. 2 Crystallite size and texture coefficient of the (002) peak for Li-ZnO thin films for different doping contents

Fig. 3 SEM images of ZnO films for various Li doping contents: **a** undoped; **b** 5% Li; **c** 10% Li; **d** 20% Li
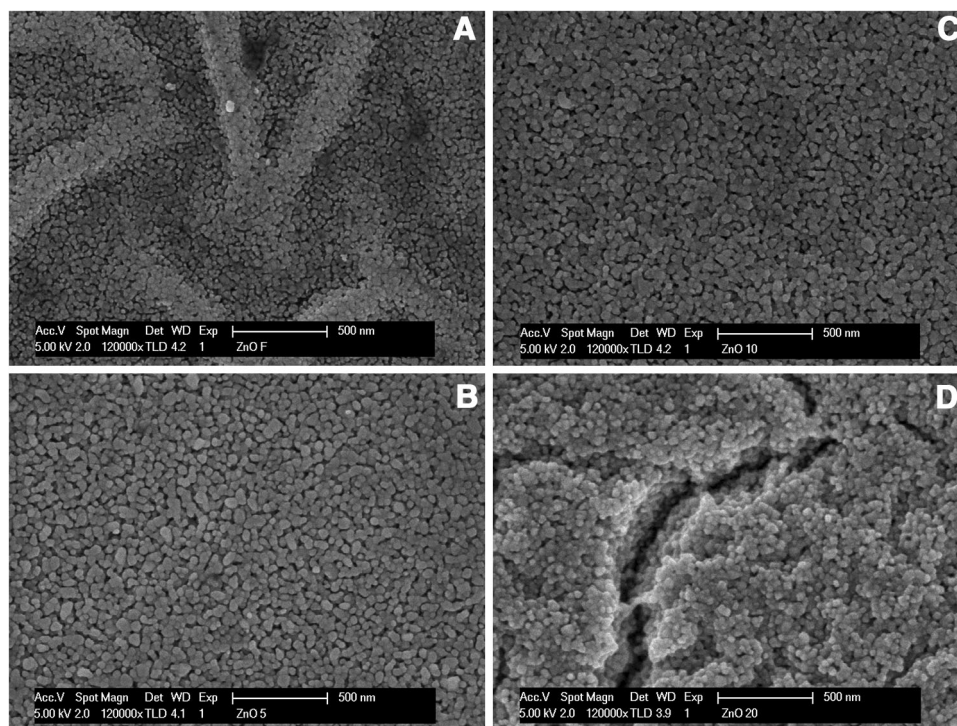

Figure 3 shows the SEM images of the surface morphology of undoped and lithium-doped ZnO thin films. We can see that the morphology evolves considerably after doping the sample. All films had a close-packed morphology with grain sizes as 60 nm.

From those images, it is observed that the doping up to 12% has little influence on the morphological surface. The samples show dense morphology without visible voids and defects overall the surfaces. When the Li content exceeds 12%, some cracks appear and many voids were found, reflecting a degradation of the film's crystallinity. This result is in good agreement with DRX data and affirms once again an improvement in the films crystallinity for doping below 12% and a marked deterioration beyond this value. Wang et al. [23] reported the same result for Li-doped ZnO and Papadimitriou [24] for Al-doped ZnO.

3.2 Optical properties

The optical transmittance measurements are a well-established method to study the optical properties of transparent conducting oxides. Optical transmittance spectra of undoped and Li-doped ZnO thin films are shown in Fig. 4. All films exhibit a high transparency in the visible region with a sharp fundamental absorption edge at about 380 nm. The average transmittance was increased after doping ZnO with Li, which is in good agreement with DRX and SEM results. The film with Li doping content at 12% show slightly higher transprency than other films. The improved
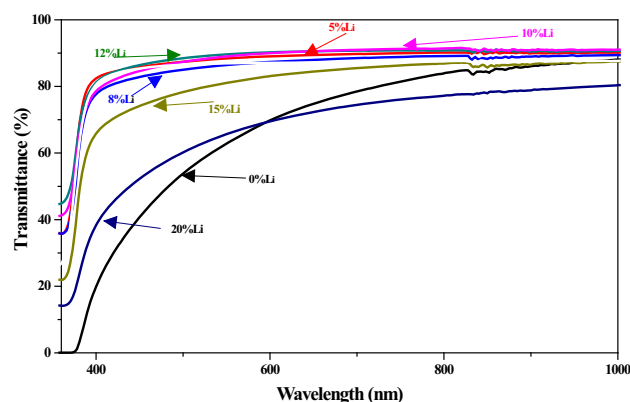

Fig. 4 Transmission spectra vs. wavelength for undoped and Li-ZnO thin films at different doping contents

transmittance up to 12% of Li concentration is associated with high crystallinity and the degradation of transmittance for heavily doping is due to a deterioration of crystallinity of samples. Generally, the change in the transparency is mainly due to transition of electrons between valence band and defect levels. These results will be approved by the band gap values described below.

The optical band gap of the films was calculated from the transmittance spectra employing Tauc plot (Eq. 1):

$$(\alpha h\nu)^2 = A(h\nu - E_g), \tag{1}$$

where A is a constant, $h\nu$ is the excitation energy and α is the absorption coefficient.
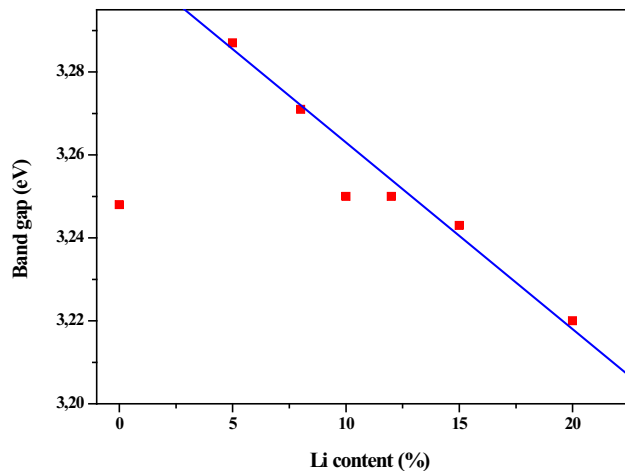
Fig. 5 ZnO optical band gap vs. Li doping content

Figure 5 shows the calculated band gap variations with the Li content. Undoped ZnO sample, exhibits a band gap values of 3.247 eV, which increases with increasing Li doping concentration up to 5% (3.286 eV), followed by a decrease for higher doping content. In this work, the decrease of optical band gap is expressed in terms of Li doping concentration (x) by the formula (Eq. 2):

$$E_g(x) = -0.0045 \cdot x + 3.31. \tag{2}$$

The same behavior was reported by Xu et al. [25] for K-doped ZnO and by Wang et al. [26] for Na-doped ZnO. The first increase of band gap can be explained by Burstein–Moss effect [27]. Therefore, the optical band gap of doped films is broader than pure ZnO films [28]. Indeed, it is well known that intrinsic defects such as Zn interstitials and O vacancies act as donor defects [29, 30]. Based on theoretical calculations performed using the first-principles pseudopotential method, Park et al. [31] had predicted that Li prefers interstitial sites to substitutional sites in ZnO and behaves as a shallow donor. Since ZnO is intrinsically n-type, it therefore has the effect of increasing the carrier concentration and hence the gap through an increasing of the Fermi level.

The linear decreases of band gap energy with the doping content can be explained by combined effects of both the formation of tails band for strong doping, and the stress caused by the change of lattice parameter. Wang et al. [26] and Bahsi et al. [32] had reported that the band tails occurring for large doping lead to absorption shifts to longer wavelengths. Zamiri et al. [33] also related the possible reason for the decrease in optical band gap to the change in defect concentration.

The in-plane stress of the films was calculated following the bi-axial model formula [34]:

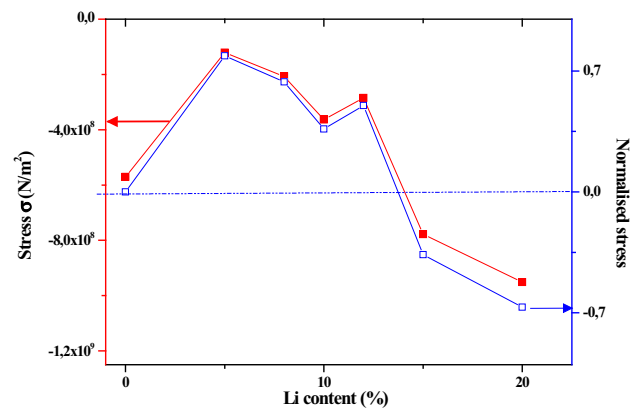$$\sigma = 4.5 \times 10^{11} \frac{c_0 - c}{c_0}, \tag{3}$$

Fig. 6 Stress and normalized stress vs. Li doping content

where c_0 is the lattice parameter of bulk ZnO (5.2066 Å) and c the corresponding values for studied films.

Figure 6 shows that σ is always negative indicating that the films are in a state of compressive nature. Most surprising here is the similarity between this behavior and that of the band gap energy. Indeed, σ depends on the Li doping content in a manner similar to that of the E_g, and therefore a correlation between E_g and σ is to be taken into account. At low doping concentration, the stress increases with the doping level. This normal evolution is due to the occupation of interstitial sites. By studying the effect of stress on optical band gap of ZnO obtained by spray pyrolysis, Prasada et al. [35] reported that the compressed lattice is expected to provide a wider band gap because of the increased repulsion between the oxygen 2p and the zinc 4s bands. On the other hand, the decrease of σ beyond a specific amount of Li doping is performed by saturation of the interstitial sites forcing Li ions to occupy substitutional ones. Park et al. [31], and Lee et al. [36] had demonstrated that substitutional Group-I elements behave as a shallow acceptor. This shallowness of acceptor levels of Li_{Zn} was attributed to the reduction of strains around the doping atoms and coupling between the anion and the cation orbitals. Finally, the reduction of stress leads to the decrease of the band gap energy.

In order to identify the doping effect on the stress by comparing the case of undoped sample to doped ones, we have calculated the normalized stress ($\sigma_{doped} - \sigma_{undoped}$)/$\sigma_{undoped}$ (Fig. 6). The result is even more surprising. Not only there is a simple shift of the curve, which is normal, but also as for XRD and SEM, two doping regions appear. In the lower doping region up to 12%, the films are in tension while for a highly doped region, a compression is obtained. This finding clearly demonstrates the important role played by the constraints on both, structural and optical properties of these layers.

4 Conclusion

Undoped and Li-doped ZnO thin films were prepared by the sol–gel method and deposited on glass substrates by spin-coating technique. The Li doping content effect on the structural, morphological, properties, and stress was found to be significant. The structural and morphological studies revealed that all films are polycrystalline and exhibit a preferential growth orientation along the *c*-axis orientation for Li doping concentration up to 12%. For further increase of Li content, a marked degradation of the film's crystallinity was observed. This behavior was confirmed by optical measurements where the optical transmission has improved initially and then decreased when the Li doping content exceeded 12%. The band gap was found to decrease nearly linearly in a wide range of Li doping contents. A correlation between the band gap variations and the stress was discussed.

The produced Li-ZnO thin films up to 12% may be useful for specific applications in solar cells for sensor devices where large surface areas are needed.

References

1. Y.C. Liu, S.K. Tung, J.H. Hsieh, Cryst. Growth **287**, 105–111 (2006)
2. A. Kassis, M. Saad, Sol. Energy Mater. Sol. Cells **80**, 491 (2003)
3. N. Ito, Y. Sato, P.K. Song, A. Kaijio, K. Inoue, Y. Shigesato, Thin Solid Films **496**, 99–103 (2006)
4. J.T. Lim, C.H. Jeong, A. Vozny, J.H. Lee, M.S. Kim, G.Y. Yeom, Surf. Coat. Technol. **201**, 5358–5362 (2007)
5. M.P. Lu, J.H. Song, M.Y. Lu, M.T. Chen, Y.F. Gao, L.J. Chen, Z.L. Wang, Nano Lett. **9**(2009), 1223–1229 (2009)
6. S. Majumdar, P. Banerji, Sens. Actuator B Chem. **140**, 134–138 (2009)
7. Q. Ahsanulhaq, J.H. Kim, J.S. Lee, Y.B. Hahn, Electrochem. Commun. **12**, 475–478 (2010)
8. S.J. Pearton, D.P. Norton, K. Ip, Y.W. Heo, T. Steiner, Superlattices Microstruct. **34**, 3–32 (2004)
9. C. Klingshirn, R. Hauschild, H. Priller, M. Decker, J. Zeller, H. Kalt, Superlattices Microstruct. **38**, 209–222 (2005)
10. T. Minami, T. Yamamoto, T. Miyata, Thin Solid Films **366**, 63–68 (2000)
11. B.M. Ateav, A.M. Bagamadova, V.V. Mamedov, A.K. Omaev, Mater. Sci. Eng. B **65**, 159–163 (1999)
12. X.W. Sun, H.S. Kwok, J. Appl. Phys. **86**(1), 408–411 (1999)
13. A. El Hichou, M. Addou, J. Ebothé, M. Troyon, J. Lumin. **113**, 183–190 (2005)
14. X. Sun, Z. Deng, Y. Li, Mater. Chem. Phys. **80**, 366–370 (2003)
15. S. Fujihara, C. Sasaki, T. Kimura, J. Eur. Ceram. Soc. **21**, 2109 (2001)
16. D.M. Cabe, K. Johnston, M.O. Henry, E. Mc Glynn, E. Alves, J.J. Davies, Phys. B **351**, 227 (2004)
17. D.Y. Wang, J. Zhou, G. Liu, J. Alloy. Compd. **481**, 802–805 (2009)
18. S. Majumdar, P. Banerji, Superlattices Microstruct. **45**, 583–589 (2009)
19. B. Xiao, Z. Ye, Y. Zhang, Y. Zeng, L. Zhu, B. Zhao, Appl. Surf. Sci. **253**, 895–897 (2006)
20. G.A. Mohamed, E.-M. Mohamed, A. Abu El-Fadl, Phys. B **308–310**, 949–953 (2001)
21. K. Meziane, A. El Hichou, A. El Hamidi, M. Mansori, A. Liba, A. Almaggoussi, Superlattices Microstruct. **93**, 297–302 (2016)
22. S.D. Senol, M. Erdem, Ceram. Int. **42**, 10929–10934 (2016)
23. D.Y. Wang, J. Zhou, G.Z. Liu, Alloys Compd. **481**, 802–805 (2009)
24. D.N. Papadimitriou, Thin Solid Films **605**, 215–223 (2016)
25. L.H. Xu, X.Y. Li, J. Yuan, Superlattices Microstruct. **44**, 276–281 (2008)
26. L.W. Wang, F. Wu, D.X. Tian, W.J. Li, L. Fang, C.Y. Kong, M. Zhou, Alloys Compd. **623**, 367–373 (2015)
27. Y.E. Jeong, S. Park, Curr. Appl. Phys. **14**, 30–33 (2014)
28. Z. Pan, X. Tian, W. Shoukun, Y. Xia, Z. Li, J. Deng, C. Xiao, H. Guanghui, Z. Wie, Appl. Surf. Sci. **265**, 870–877 (2013)
29. S.B. Zhang, S.H. Wie, A. Zanger, Phys. Rev. B **63**, 075205 (2001)
30. C. Ravichandran, G. Srinivasan, C. Lennon, S. Sivanathan, J. Kumar, Mater. Sci. Semicond. Process **13**, 46–50 (2010)
31. C.H. Park, S.B. Zhang, S.H. Wie, Phys. Rev. B **66**, 073202 (2002)
32. Z.B. Bahsi, A.Y. Oral, Opt. Mater. **29**, 672–678 (2007)
33. R. Zamiri, A.F. Lemos, A. Reblo, H.A. Ahangar, J.M.F. Ferreira, Ceram. Int. **40**, 523 (2014)
34. J. Lai, Y.J. Lin, Y.H. Chen, H.C. Chang, C.J. Liu, Y.Z. Zou, Y.T. Shih, M.C. Wang, J. Appl. Phys. **110**, 013704 (2011)
35. T. Prasada Rao, M.C. Santosh Kumar, S. Anbumoshi Angayarkanni, M. Ashok, J. Alloy Compd. **485**, 413–417 (2009)
36. E.C. Lee, K.J. Chang, Phys. Rev. B **70**, 115210 (2004)